Analyst

ROYAL SOCIETY OF CHEMISTRY

PAPER

View Article Online
View Journal | View Issue

Check for updates

Cite this: *Analyst*, 2021, **146**, 4268

A new metric for relating macroscopic chromatograms to microscopic surface dynamics: the distribution function ratio (DFR)†

Logan D. C. Bishop, [a] Anastasiia Misiura [a] and Christy F. Landes *[a,b,c,d]

Heterogeneous stationary phase chemistry causes chromatographic tailing that lowers separation efficiency and complicates optimizing mobile phase conditions. Model-free metrics are attractive for assessing optimal separation conditions due to the low quantity of information required, but often do not reveal underlying mechanisms that cause tailing, for example, heterogeneous retention modes. We report a new metric, which we call the Distribution Function Ratio (DFR), based on a graphical comparison between the chromatogram and Gaussian cumulative distribution functions, achieving correspondence to ground truth surface dynamics with a single chromatogram. Using a Monte Carlo framework, we show that the DFR can predict the prevalence of heterogeneous retention modes with high precision when the relative desorption rate between modes is known, as in during surface dynamics experiments. Ground truth comparisons reveal that the DFR outperforms both the asymmetry factor and skewness by yielding a one-to-one correspondence with heterogeneous retention mode prevalence over a broad range of experimentally realistic values. Perhaps of more value, we illustrate that the DFR, when combined with the asymmetry factor and skewness, can estimate microscopic surface dynamics, providing valuable insights into surface chemistry using existing chromatographic instrumentation. Connecting ensemble results to microscopic quantities through the lens of simulation establishes a new chemistry-driven route to measuring and advancing separations.

Received 2nd March 2021,
Accepted 1st June 2021

DOI: 10.1039/d1an00370d

rsc.li/analyst

Published on 02 mis Metheven 2021. Downloaded on 31/05/2026 19:36:48.

1. Introduction

Understanding the microscopic surface mechanisms underlying chromatographic separations is crucial for moving drug production from quality by testing[1] to quality by design.[2] Doing so would help reduce the purification and separation cost of new protein pharmaceuticals as well as alleviate the energy burden induced by industrial separations.[3–5] Recent efforts to move towards separations-by-design include novel column designs, continuous flow systems, new single-analyte measurements, advanced statistical analysis, and mechanistic simulations and theory.[1,6–10,12–19,42] It is thus possible to correlate microscopic phenomena to ensemble observables such as chromatographic elution curves. Most discussions of tailing address column overloading,[19–21] but tailing can also occur due to rare, heterogeneous interactions with the stationary phase surface. Surface heterogeneity can be introduced by surface defects[7,9] or result from specific *versus* non-specific binding,[11] an effect often seen in chiral separations.[22] Ideally, we also need new methods to extract mechanistic details from macroscopic separation observables.

Detailed chemical information is captured in the lineshape of a chromatogram. Lineshape analysis can infer the number of adsorption events in the column,[23] varied adsorption kinetics,[24] non-linear column contributions,[25] and flow effects.[26,27] Other methods rely on analytical models that approximate the curve using variables without physical meaning,[27,28] fitting peaks based on analytical series,[29] or need ancillary equipment during data collection.[30,31] Conversely, model-less metrics using only the chromatogram have been utilized to interpret microscale phenomena and are common metrics for separation optimization[32,33] but rarely can relate changes in chromatogram shape to changes in stationary phase surface chemistry. Here, a disconnect forms between relating the results of an ensemble separation performed in a column measured in millimeters to microscopic details measured over

[a]*Department of Chemistry, Rice University, Houston, Texas 77251, USA. E-mail: cflandes@rice.edu*
[b]*Department of Electrical and Computer Engineering, Rice University, Houston, Texas 77251, USA*
[c]*Department of Chemical and Biomolecular Engineering, Rice University, Houston, Texas 77251, USA*
[d]*Smalley-Curl Institute, Rice University, Houston, Texas 77251, USA*

†Electronic supplementary information (ESI) available. See DOI: 10.1039/d1an00370d

This journal is © The Royal Society of Chemistry 2021

Published on 02 mis Metheven 2021. Downloaded on 31/05/2026 19:36:48.

micrometers of stationary phase surface, such as those captured in single-molecule studies.[34–36] Recently, we demonstrated that the most popular graphical metric, the asymmetry factor (A_s), is not suitable for microscale studies of surfaces due to non-linear relationships with respect to rare retention mode statistics and underestimation of the amount of analyte lost in the tail.[37] Development of a graphical metric that infers surface chemical effects from ensemble chromatograms would translate decades of opaque experimental optimization into powerful observations of chemical phenomena occurring on the stationary phase surface.

The Distribution Function Method (DFM)[38–40] detects peak variations by comparing two distributions in a parametric plot, providing qualitative proof of minute deviation, but lacking correlation to an underlying mechanism. Repurposing the DFM to create trackable phenomena can correlate chromatogram lineshape to ground truth physical chemistry at the surface, like mixed-mode adsorption[41] and stationary phase hopping,[42] from ensemble data alone. Pivoting to include mobile phase simulations could extend correlations to mobile phase artifacts from flow[43,44] and column structure,[45–49] extra column components and injection methods,[50–52] and diffusion within pores.[53–56] Correlation of simulated effects with chromatogram lineshape provides a necessary bridge between macroscale and microscale measurements.[57,58]

In this work, we expand the DFM as a ratio of the chromatographic cumulative distribution function (CDF) and a Gaussian CDF, a method we call the Distribution Function Ratio (DFR), to calculate microscopic surface dynamics from a single chromatogram. Comparisons to a Gaussian lineshape improve upon Rix's original method by eliminating the need for ancillary peaks to characterize the chromatogram.[39] Further, chromatogram lineshape is shown to correlate pseudo-linearly to mixed-mode adsorption dynamics, capturing important surface statistics using only the ensemble chromatogram. Mixed-mode adsorption dynamics, a model for kinetic tailing in low dilution and topic of interest for pharmaceutical separations,[59,60] is used to simulate chromatograms from ground truth statistics and demonstrate the utility and precision of the DFR. Here, we show that the DFR outperforms A_s and statistical skewness over a wide range of relative prevalence and relative desorption rate of rare, high energy, slow desorbing retention modes on the stationary phase surface. Use of the DFR with microscale surface information provides high precision estimates of surface retention modes. However, in absence of microscale surface insight, A_s and skewness can be used in combination with the DFR to estimate surface dynamics from the ensemble peak alone. The DFR is used to analyze a separation of a model protein, lysozyme, capturing valuable statistics about surface retention modes. Combining the DFR with ground truth simulations generates calibration curves that connect peak shape to surface physicochemistry, creating an optimizable metric that interrogates stationary phase surface dynamics while reporting on the quality of separation. Using the DFR quantifies rare surface defects and specific adsorption using only ensemble chromatography.

2. Experimental section

2.1. Theory

Tracing the source of mixed-mode kinetic tailing requires knowledge of the prevalence and desorption statistics of retention modes on the stationary phase surface. We examine tailing in mixed-mode chromatography where a protein alternates between flowing in the mobile phase and surface adsorption through two different retention modes, the first mode fast desorbing and prevalent, the other slower desorbing and increasingly rare. Each retention mode has a distinct rate of desorption (k_j) and expected desorption time ($\langle\tau_j\rangle$) that describes an exponential distribution of singular desorption times (τ_j), where higher energy retention modes have longer expected desorption times.[61] Stationary phases with two retention modes ($m = 2$) induce tailing and broadening in chromatography,[60,62,63] though a proliferation of retention modes ($m > 2$) can exist depending on surface microstructure and functionalization.[64–67] The number of retention modes on the surface and their desorption rates can be gathered experimentally using microscale, surface measurements.[13,42] However, direct observations of surface dynamics are limited spatially, on the order of micrometers, while column lengths are on the millimeter scale. Capturing the desorption time differences between common and rare modes and correlating their prevalence to column-wide experimental parameters is critical for reducing chromatographic tailing and can only be achieved through simulation and theory.

Modeling the tailing effects of mixed-mode adsorption requires knowledge of molecular elution histories. Kinetic chromatographic tailing occurs when a small population of molecules forms a broad distribution of elution times due to interactions with a rare, high energy retention mode, even in dilute conditions where column overload does not occur.[24,63] The stochastic theory of chromatography captures rare interactions by describing molecular elution as a molecule undergoing a random walk between moments of mobility and stationarity. The elution history of each molecule is then a series of connected adsorption events sampled from available retention modes.[68] A master equation for the retention time of a single molecule (T) that incorporates interactions for every adsorption event across all retention modes is then eqn (1):

$$T = t_m + t_s = t_m + \sum_{j=1}^{m}\sum_{i=1}^{n}\tau_{i,j} \quad (1)$$

where t_m, t_s represent the sums of time spent in the mobile, stationary phase and $\tau_{i,j}$ is the length of time spent during the i^{th} adsorption event through the j^{th} retention mode.[69] Here, assumption of a constant mobile phase time (t_m) isolates the tailing contribution of heterogeneous adsorption rather than convolves it with mobile phase effects, of which there are many.[70,71] A chromatogram can be simulated by aggregating thousands of results from eqn (1) using Monte Carlo methods educated by ground truth chemical quantities found in surface

Published on 02 mis Metheven 2021. Downloaded on 31/05/2026 19:36:48.

studies, correlating retention mode energy/prevalence to different tailing metrics.[72]

The molecular histories produced by the Monte Carlo simulations are random samples of the "frequency functions" described by Dondi.[73,74] Analytically, each frequency function is the sum of all n^{th} fold convolutions of the distribution of the retention mode desorption times over n adsorption/desorption steps for $0 \leq n \leq \infty$. For the homogeneous case, the stationary phase time, $c_s(t)$:

$$c_s(t) = \sum_n P(n) f_{s,1}(\tau)^{n*} \quad (2)$$

where $P(n)$ is the probability of a molecule undergoing n adsorption/desorption steps, $f_{s,1}(\tau)$ is the distribution of desorption times for the common mode, and $n*$ is the n^{th} fold convolution. For the heterogeneous two-retention mode case, the equation can be expanded to eqn (3) for $0 \leq n \leq \infty$, per Cavazzini:[60]

$$c_s(t) = \sum_n P(n) f_{s,1}(\tau)^{n*} + \sum_n P(n) \sum_{j=0}^{n-1} \binom{n}{j} p^j (1-p)^j f_{s,1}^{j*}(\tau) * f_{s,2}^{(n-j)*}(\tau) \quad (3)$$

where $\binom{n}{j} p^j (1-p)^j$ is the Bernoulli coefficient for j interactions with the common retention mode with relative prevalence p out of n total adsorption/desorption steps and $f_{s,2}(\tau)$ is the distribution of desorption times for the rare retention mode. Monte Carlo simulations avoid convolutions by directly calculating the sum of random variables over n adsorption/desorption steps, constructing the distributions in $c_s(t)$ through random sampling. As such, we define $c_s(t)$ non-analytically as a mixture model[75] of our Monte Carlo calculated molecular history distributions where each distribution is differentiated by the number of interactions with a rare retention mode (eqn (4)):

$$c_s(t) = \alpha_1 f_1(t) + \alpha_2 f_2(t) + \sum_{i=3}^{m} \alpha_i f_i(t) \quad (4)$$

where $f_i(t)$ are the distributions of molecular retention times that have interacted with the i^{th} rare retention mode and α_i represent the fraction of molecular histories sampled from the i^{th} subpopulation and must sum to 1. Here, $f_1(t)$ describes the homogenous distribution of molecular histories, equivalent to eqn (2), and $f_2(t)$ is equivalent to the second term in eqn (3). The third term of eqn (4) includes any additional modes past the first rare mode. In transitioning from eqn (3) to eqn (4), we have released the requirement that n be strictly known in favor of functions that can be analyzed by profile shape. The visual result of eqn (4) is presented in Fig. S1.† To utilize eqn (4) in our analysis, we have assumed that the mobile phase contribution has been removed by deconvolution with the distribution of an unretained tracer analyte.[23,79] Contributions to t_m include flow heterogeneity due to stationary phase structural imperfections and extra-column factors, both leading to asymmetry or broadening.[76–78] The long column approximation guarantees that the homogeneous population forms a Gaussian ($f_1(t) \approx g(t)$) when a sufficient number of adsorption events have occurred and is often considered the ideal peak shape.[14,33] However, achieving the Gaussian limit when heterogeneous adsorption is present requires columns not usually seen in practice.[80] Several studies have shown that comparisons to a Gaussian can quantify asymmetry of the lineshape[81,82] or estimate sub-resolution curves when proper assumptions are made.[83] Combining eqn (4) and the long column approximation establishes that any deviations from the Gaussian lineshape carry information about the tailing distributions $\sum_i^m f_i(t)$. Quantifying deviations from the Gaussian distribution is then an avenue to measure statistics of the tailing distributions in the chromatogram lineshape without specifying an analytical model for each distribution $f_i(t)$.

2.2. Metric definition

Methods developed from the DFM[38,39] can detect small deviations in the lineshape of two distributions while remaining tolerant to excessive experimental noise.[38] Briefly, the DFM qualitatively differentiates two distributions (Fig. 1A) by comparing the shape of each chromatogram's CDF (Fig. 1A, inset) normalized to the time interval (0,1) through the function $\theta(t)$ (see ESI†), and abbreviated as θ when used as a variable. Our

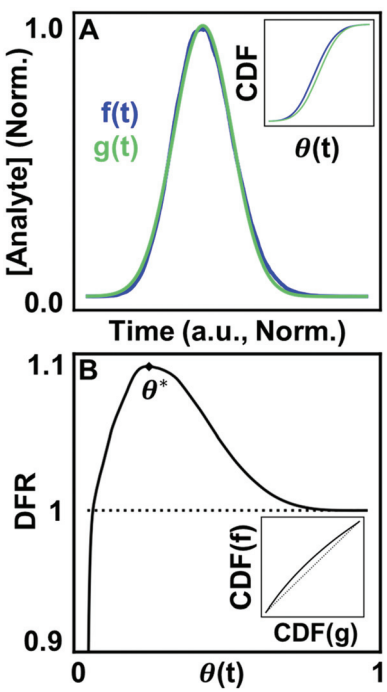

Fig. 1 Utilizing CDFs to detect differences between chromatograms and the Gaussian lineshape. (A) A simulated chromatogram overlaid with a Gaussian curve. (Inset) CDFs of each curve graphed in normalized time. (B) The DFR comparing both curves with the quantity of interest, DFR peak position (θ*), annotated. (Inset) Rix's parametric DFM comparison for both curves.[38]

 This journal is © The Royal Society of Chemistry 2021

Published on 02 mis Metheven 2021. Downloaded on 31/05/2026 19:36:48.

modification of the DFM always compares to a Gaussian CDF, adopting the Gaussian as the 'ideal' chromatogram through the posing of eqn (4). Further, taking the ratio of both CDFs generates trackable peak phenomena, providing quantitative tracking of underlying physical chemistry rather than qualitative acknowledgment of the difference of two chromatograms, as in Rix's original work. Mathematically, the DFR for any chromatogram/Gaussian pair ($c(\theta)$, $g(\theta)$) is then the ratio of their CDFs (see ESI†) over the normalized time interval θ (eqn (5)):

$$\mathrm{DFR}(0 < \theta \leq 1; c(\theta), g(\theta)) = \frac{\int_0^\theta c(t)\mathrm{d}t}{\int_0^\theta g(t)\mathrm{d}t} = \frac{C(\theta)}{G(\theta)} \quad (5)$$

The result of eqn (5) is a unique, characteristic curve for every chromatogram (Fig. 1B) with a critical value in the form of peak position (θ^*). Generating quantitative, optimizable peak phenomena differentiates the DFR from the original DFM result (Fig. 1B, inset), which only qualitatively assesses if two distributions are different through deviations along the diagonal. As such, two separate chromatograms are needed to quantify chemical effects in a single experiment. The DFR retains the benefits of Rix's original method in only utilizing the chromatogram lineshape without fitting to a model but extracts chemical information through comparison to the Gaussian curve normalized in time and concentration, avoiding the need for a second chromatogram. Normalization also minimizes the contribution of broadening by the mobile phase (Fig. S2†), further isolating the stationary phase contributions. Because deviations from a Gaussian represent contributions due to heterogeneous surface interactions, per eqn (4), information about the tailing distributions is captured in the DFR lineshape. Ground truth simulations correlate the energy and prevalence of rare retention modes to the chromatogram lineshape and validate that the DFR can capture statistics of tailing distributions. The DFR provides an estimate of the relative column prevalence of a retention mode identified through microscale surface measurements, bridging the spatial difference between surface dynamics measurements (μm scale) and the full-length column (mm scale). Further, estimating microscopic surface dynamics from the ensemble chromatogram alone provides a no-cost evaluation of the need for more complex, micrometer resolution experiments.

2.3. Computational details

Chromatographic simulations were performed using a Monte Carlo framework programmed in Python 3 programming language[84] (Python Software Foundation, https://www.python.org/) using Numpy[85] and Scipy.[86] The simulation framework is based on the work of Dondi[14] and Cavazzini,[13] and detailed in our previous publications.[38,42] The benefits of the Monte Carlo framework is that it is agnostic towards retention mechanisms when the mathematics are properly posed and is the only route for modeling non-linear chromatography.[87,88] Surface crowding is not included in the simulations, meaning that all chromatographic artifacts are the product of kinetic tailing rather than thermodynamic column overloading. Therefore, changes measured with the DFR only relate to surface kinetic effects, a connection unachievable experimentally and only partially realized in microscale surface experiments without simulation. The simulations treat time and distance as abstract, unitless quantities that are adaptable to any column length or surface chemistry. Time is measured in the unitless value δt, which adapts to the units of the kinetic rate for the retention mode.[89] Our Monte Carlo simulation framework treats each molecular elution as a random walk down a connected series of column 'slices', where the slice width is the expected travel distance between transitions in the mobile-stationary phase interface. Elution speed is set such that each molecule takes $1\delta t$ to traverse a column slice. For the simulations in this work, the simulated column has 1000 column slices with a constant mobile phase time $t_m = 1000\delta t$. The number of slices correlates to the difference in linear distance between a wide-field microscope field of view (~32 μm) and a real column (~30 mm).

Adsorption events are simulated using statistical sampling parameterized by the probability of interaction with the stationary phase surface, the probability of encountering a specific retention mode (p_j), and the expected desorption time of that retention mode ($\langle\tau_j\rangle$). A schematic for the random walk a molecule undergoes in each slice is shown in Fig. 2. Here, we assume each molecule has a probability ($p_a = 0.5$) of undergoing adsorption exactly once within each slice. The probability of interaction with the surface is arbitrarily chosen but operates as a tunable parameter adjusted to fit available surface dynamics data. The original stochastic theory assumes that an average probability is satisfactory if a molecule fluctuates through the range of adsorption probabilities many times between adsorptions.[68] Further, Hlushkou *et al.* have described the probability of adsorption upon interaction with the surface as a constant based upon geometrical and energetic consideration for the adsorption process.[89,90] However, we note

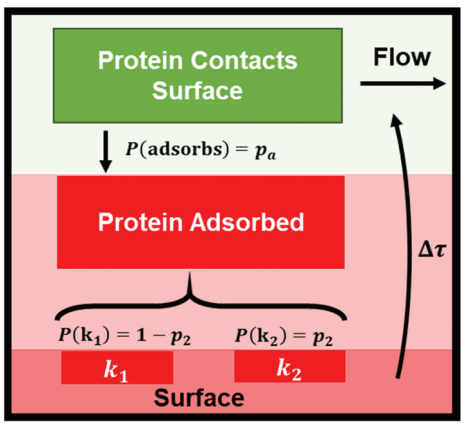

Fig. 2 A graphical depiction of a simulated column 'slice' showing the probabilistic decision branches to simulate interactions with the stationary phase. A protein encounters the surface, undergoes adsorption with some probability (p_a), and adsorbs to the surface through one of j retention modes with a likelihood of selection p_j. Each mode has a distinct rate of desorption k_j. Figure modified with permission from ref. 37. Copyright Elsevier 2020.

Published on 02 mis Metheven 2021. Downloaded on 31/05/2026 19:36:48.

that our probability is conditioned on the phase ratio of the column and could be expanded to include local heterogeneity of the stationary phase surface. Including local fluctuations in probability in the model framework is a natural extension as more experimental information becomes available.

Each slice can be considered a column feature, such as a bead, similar to the description provided by Horvath *et al.*[91] The 'surface' of each slice has m retention modes, each with some probability of selection (p_j). In the case of our simulations, the probability of interacting with the low energy, faster desorbing retention mode is higher than interaction with high energy, slower desorbing retention mode ($p_1 \gg p_2$). After retention mode selection, a desorption time ($\Delta\tau$) is sampled from an exponential distribution parameterized on the desorption rate constant (k_j) of the retention mode ($e^{-\tau k_j}$) with expected desorption time of $\langle\tau_j\rangle = \frac{1}{k_j}$.[23,61] Simulating many molecules down the column and aggregating the elution histories together generates a chromatogram.

2.4. Experimental methods

The chromatographic experiments were carried out using a home-built Fast Protein Liquid Chromatography (FPLC) system. Protein solutions of 8.3 μM Lysozyme from chicken egg white (>98%; Sigma) in the presence of 1 M sodium chloride (NaCl) were prepared in 10 mM HEPES buffer (Sigma, pH 7.2). All the solutions were injected into the FPLC using a 1 mL syringe (Becton Dickinson) with an injection volume of 300 μL. A constant flow of 2 ml min^{-1} was controlled using a peristaltic pump (Watson-Marlow, 120 Series). Absorbance from the analyte was monitored at 280 nm using a UV detector (Spectrum Chromatography). The signal then was converted from current to voltage by a digital recorder (Hantek, 365E) controlled by Hantek 365 software that registered the output signal. The syringe hydrophilic filters with polyvinylidene fluoride (PVDF) membranes (hydrophilic 0.45 μm pore size, 25 mm diameter) and hydrophobic filters with PVDF membranes (hydrophobic 0.45 μm pore size, 25 mm diameter) used as chromatographic media were purchased from Cole-Parmer and Sigma Aldrich, respectively. A series of three connected PVDF syringe filters were assembled and integrated with the setup. All components of the FPLC system were connected using silicone tubing (MED-X.D., 0.063″ internal diameter).

2.5. Computational details

A two-mode system was simulated using four different ratios of desorption rates over a range of strong retention mode prevalence. The common, low energy retention mode has an expected desorption time of $\langle\tau_1\rangle = 4\delta t$, equivalent to four times as long as necessary to traverse the column slice. Expected desorption times of the rare, high energy retention mode are then a factor longer than the expected desorption times of the common, low energy retention mode $\left(\frac{\langle\tau_2\rangle}{\langle\tau_1\rangle} = 5, 25, 50, 125\right)$ over a range of relative prevalence ($10^{-5} \leq p_2 \leq 10^{-2}$) covering several orders of magnitude. Relative prevalence is defined with respect to the number of slices in the column. Here, the relative prevalence relates to the absolute number of times a molecule interacts with a rare site ($0.01 \leq (i_{m=2}) \leq 10$). Each simulation consisted of 300 000 simulated molecules, which was shown to be sufficient for stabilization of the curve shape (Fig. S3†). The distribution of adsorption events per molecule (n) forms a Gaussian about $\langle n\rangle$ = 500 given a 50% chance of adsorbing to the surface in a 1000 slice column. The average number of adsorption–desorption events as well as the chance of adsorbing to the stationary phase can be validated through peak analysis of ensemble data.[13,23] Adjusting the probability of adsorption (p_a) and the number of slices will change the value of n and therefore the shape of the chromatogram. However, previous studies with similar theories and models have extracted useful information from a small number of interactions and discussed methods for scaling the profile in terms of the average number of adsorption events.[13,14,73,92] Simulated molecule histograms are smoothed with a Savitzky–Golay filter before cubic splining, producing the final chromatographic curve used for analysis (Fig. S4†).[93,94]

Functions that are used in the DFR must be normalized in time and concentration. The time domain is normalized using the function $\theta(t)$ beginning/ending when the signal passes above/below a defined percent of the peak height. The recovered mass within those bounds is normalized to one $\left(\int c_s(\theta(t))dt = 1\right)$. The bounds chosen for each sample are 1% of the max height of $c_s(t)$. The shape of $c_s(t)$ is compared to a Gaussian distribution in θ with the mean at θ = 0.5. Normalization of time and mass generates the same Gaussian curve for any chromatographic peak making any form of peak fitting unnecessary. Bounds for the Gaussian CDF $\left(G(\theta) = \int g(\theta)d\theta\right)$ is set to 1.5% the max height of the representative Gaussian. How bound selection changes the shape of $G(\theta)$ (Fig. S5A†) and the percent of the curve that falls outside the bounds (Fig. S5B†) are shown in the ESI. DFR peak position (θ^*) is found using the first derivative test.

4. Results and discussion

4.1. Extracting relative desorption rate and high energy retention mode prevalence using the DFR

Curvature changes in the chromatographic lineshape encode information about the relative prevalence of stronger retention modes at the stationary phase surface and are extractable by tracking the DFR peak position (θ^*). Fig. 3 compares the sensitivity of θ^* and A_s to changes in the prevalence of the high energy retention mode (p_2) at several relative desorption rates $\left(\frac{\langle\tau_2\rangle}{\langle\tau_1\rangle} = 25, 50, 125\right)$. At minor differences in desorption rates, low enough that chromatographic peaks are visually similar (Fig. 3A), θ^* still detects surface heterogeneity at low levels of prevalence and can differentiate between prevalence with high precision (Fig. 3B). A_s does not share the traits of sensitivity or differentiability, reporting homogeneity at low prevalence and

 This journal is © The Royal Society of Chemistry 2021

Published on 02 mis Metheven 2021. Downloaded on 31/05/2026 19:36:48.

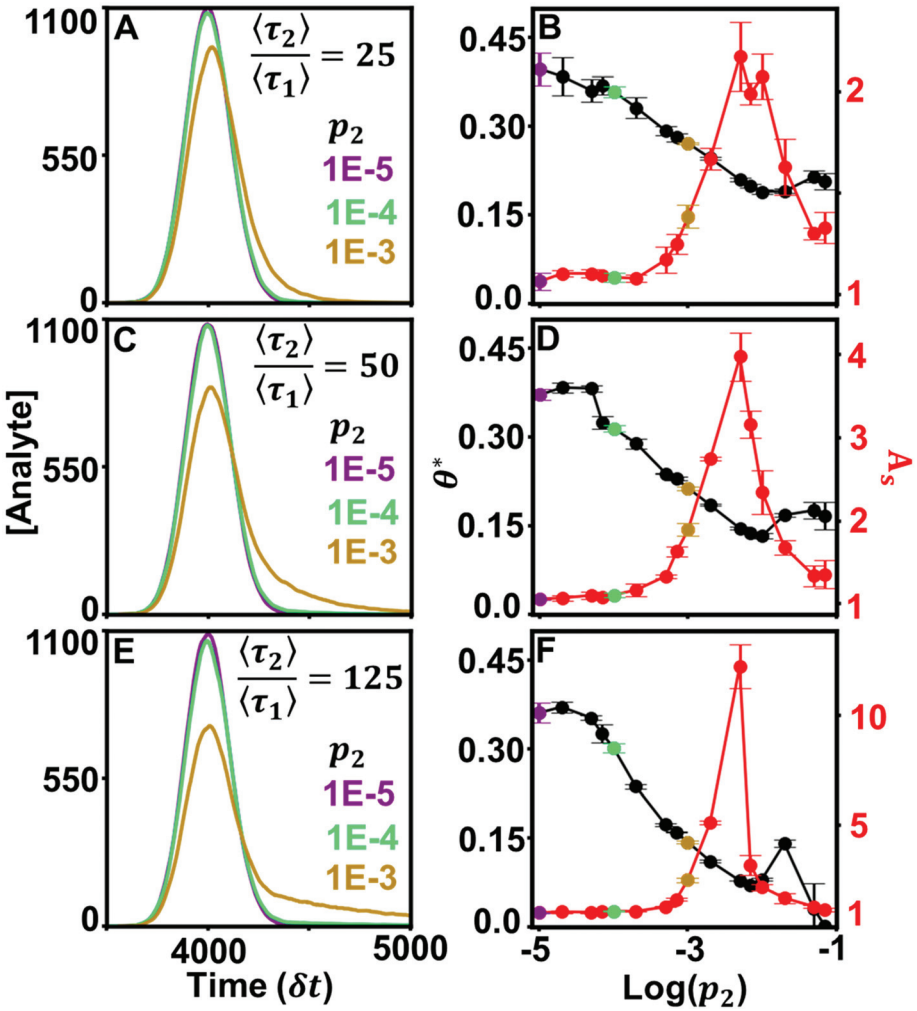

Fig. 3 Simulated chromatograms (left) and their calculated θ^* and A_s values (right). Average desorption time of the stronger retention mode increases across the values $\frac{\langle\tau_2\rangle}{\langle\tau_1\rangle} = 25$ (A and B), 50 (C and D), 125 (E and F).

losing predictive power through lack of one-to-one correspondence at higher prevalence. Higher desorption rate ratios $\left(\frac{\langle\tau_2\rangle}{\langle\tau_1\rangle}\right)$ of 50 (Fig. 3C/D) and 125 (Fig. 3E/F) do not diminish the precision or differentiability of the DFR or improve the results of A_s. Using A_s cannot provide an accurate assessment of surface homogeneity, even when chromatograms visually tail. Tracking θ^* provides a pseudo-linear, one-to-one correspondence over a wide range of prevalence with high precision at a variety of different retention mode energies with a single chromatogram when the ratio of desorption rates is known.

The DFR can still differentiate surface effects when the difference between retention mode desorption rates nears homogeneity. Fig. S6† examines a kinetic scenario where the ratio of expected desorption times between the low and high energy retention modes is a factor of 5. Small differences in kinetics produce chromatograms that appear symmetric and are indifferentiable by eye (Fig. S6A†). θ^* tracks the prevalence of the slow retention mode while A_s is incapable of differentiating between the peaks (Fig. S6B†). Development of custom-designed columns and stationary phases[95,96] could be advanced by a metric that can interrogate surface heterogeneity at a wide range of experimental conditions, especially near-homogeneous conditions that approximate, but do not reach, the ideal Gaussian lineshape. Implementing the DFR in tandem with surface dynamics measurements to direct the selection of macroscopic experimental parameters achieves chemistry-driven design of stationary phases.

4.2. Tracking θ^* identifies surface dynamics when other graphical metrics fail

Values of θ^* are unique for each prevalence within a desorption rate trendline but are not unique between relative desorption rates. Fig. 4 graphs all four simulated chromatogram sets for three metrics: A_s (Fig. 4A), skewness (Fig. 4B), and θ^* (Fig. 4C). Identifying surface dynamics from the ensemble measurement requires a one-to-one correspondence trend across a wide range of possible prevalence values for the rela-

Published on 02 mis Metheven 2021. Downloaded on 31/05/2026 19:36:48.

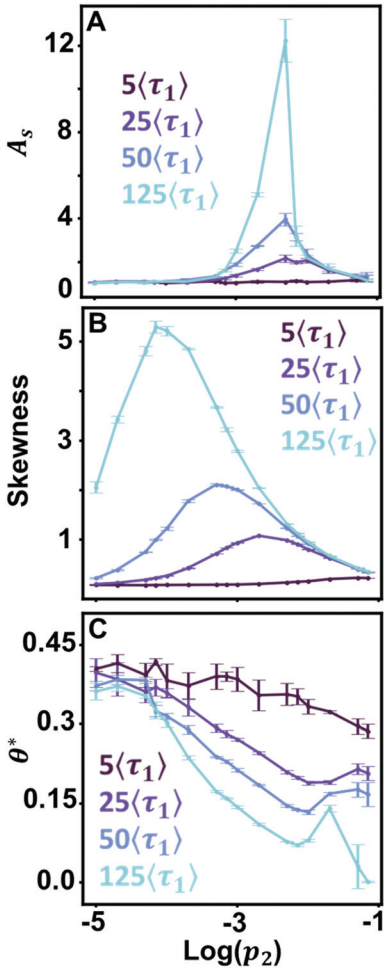

Fig. 4 Comparison of the graphical metrics of A_s (A), skewness (B), and θ^* (C) for all simulated chromatograms used in Fig. 3 and S4†.

tive desorption rate. Here, both A_s and skewness either lose sensitivity over a range of values or provide two possible prevalence even when the relative desorption rate between modes is known. Knowledge of the surface dynamics does not provide the means to correctly assess the prevalence of a retention mode in the full column. Conversely, θ^* provides a near one-to-one correspondence over several orders of magnitude, providing an optimizable metric when the relative desorption rate has been measured. Therefore, spatially limited microscale measurements of surface dynamics can extrapolate the rare retention mode prevalence across the length of the macroscale column. Complications arise when the relative desorption rates ($\langle\tau_1\rangle$, $\langle\tau_2\rangle$) are unavailable to direct selection of a θ^* trend line, such as when surface dynamics measurements have not been performed. Here, the one-to-one correspondence of θ^* no longer holds when other relative desorption rates are considered (Fig. 4C). Microscopy measurements are necessary to achieve a high precision estimate of surface dynamics, either in identifying relative desorption rate or relative prevalence of retention modes. However, aggregating several ensemble accessible metrics can educate the selection of relative desorption rate and mode prevalence.

4.3. Estimating mixed-mode prevalence and desorption rate without surface dynamics measurements

Combining θ^* with ancillary graphical metrics can estimate p_2 or $\langle\tau_2\rangle$ when information about surface dynamics is unavailable. Fig. 5 presents a workflow for estimating surface heterogeneity from ensemble information alone. As an example, we consider two chromatograms with kinetics that do not lie along trendlines presented previously (Fig. 5A). To direct selection of a θ^* trendline, other graphical information can be incorporated. Fig. 5B is a parametric plot of A_s *versus* skewness that can be used in the same manner as a phase diagram. Calculating both A_s and skewness can help estimate the value

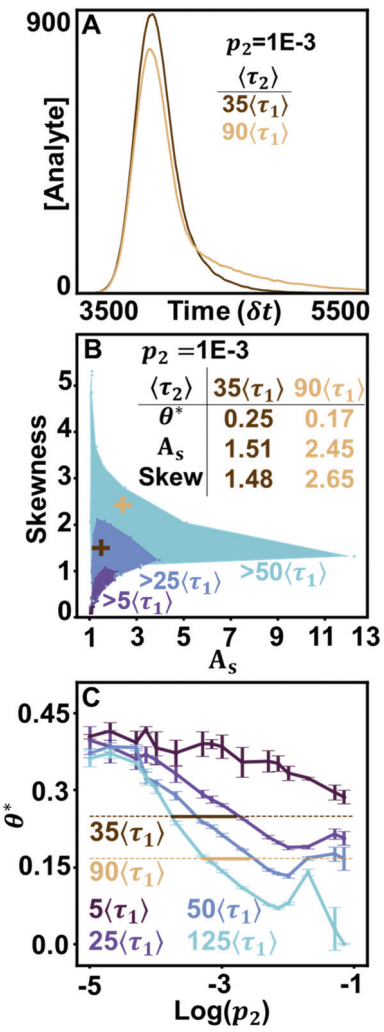

Fig. 5 Estimating surface heterogeneity from ensemble information. (A) Simulated chromatograms with kinetic rates $\frac{\langle\tau_2\rangle}{\langle\tau_1\rangle} = 35$ and 95 with p_2 = 0.001. (B) A parametric plot of A_s and skewness from Fig. 4C trendlines. Chromatograms in panel A are denoted with crosses (C) All θ^* trends with possible (dotted) and estimated (solid) solutions for simulated chromatograms from panel A.

This journal is © The Royal Society of Chemistry 2021

Published on 02 mis Metheven 2021. Downloaded on 31/05/2026 19:36:48.

of $\langle\tau_2\rangle$ from simulated data by identifying a range of valid relative desorption ratios. The values for the chromatograms in Fig. 5A are marked with crosses and correctly estimate the relative desorption rate between retention modes for both simulations. Fig. 5C illustrates possible solutions for $\langle\tau_2\rangle$ and p_2 for the simulated chromatograms given the values of θ^*. Using information provided by the parametric plot in Fig. 5B, the set of possible solutions (dotted line, Fig. 5C) is reduced to a smaller estimate set with stricter bounds (solid line, Fig. 5C). Here, we have successfully estimated the microscale surface values of $\langle\tau_2\rangle$ and p_2 from the ensemble chromatogram alone, bridging the knowledge gap through simulations.

4.4. Using θ^* to guide assessment of experimental chromatograms

Evaluating θ^* in ensemble separations connects experimental results to simulated chromatograms, enabling analysis of plausible surface chemistry. The effectiveness of profile shape analysis has been illustrated experimentally using a library of standard control curves.[97] Here, we replicate that process using simulated two-retention mode curves to estimate surface dynamics in two ensemble separations. Fig. 6 shows two real separations of lysozyme over hydrophobic and hydrophilic PVDF membranes and DFR analysis used to detect possible heterogeneity on the stationary phase surface. Fig. 6A overlays the chromatograms for lysozyme flowed over hydrophobic and hydrophilic membranes. We begin our analysis with the assumption that the chromatogram can be best explained using a two-retention mode system, a kinetic scenario well studied in theory and commonly seen experimentally on otherwise homogeneous surfaces.[9,61,65,92,98,99] Subsequent, rarer, stronger retention modes are possible but negligibly contribute to profile shape (Fig. S1†).

Fig. 6B/C present DFR analysis for the hydrophobic and hydrophilic separation, respectively, overlaying the experimental data with a simulated chromatogram that matches in θ^*. In both cases, a simulated peak was found that showed good agreement with the raw data. Peak position/height were matched to reduce differences in t_m and normalize for concentration, respectively. The time-domain was normalized to account for differences between the time resolution of the FPLC detector (0.6 ms) *versus* the simulated unit of time (δt).[88] Possible solutions for the surface kinetics are extrapolated from simulated chromatograms that closely match the experimental curve shape and the experimental value of θ^* (Tables S1 and S2†). The subset of the simulations used to extrapolate the surface kinetics are co-plotted with the experimental data in Fig. S7 and S8.†

The matching simulated chromatograms indicate that the surfaces could be described using a two-retention mode system where the rare, long binding mode has a relative desorption time of $\frac{\langle\tau_2\rangle}{\langle\tau_1\rangle} = 65$ and relative prevalence $p_2 = 0.007$ on the hydrophobic membrane and $\frac{\langle\tau_2\rangle}{\langle\tau_1\rangle} = 50$ and $p_2 = 0.01$ on the hydrophilic membrane. Previous work in the group

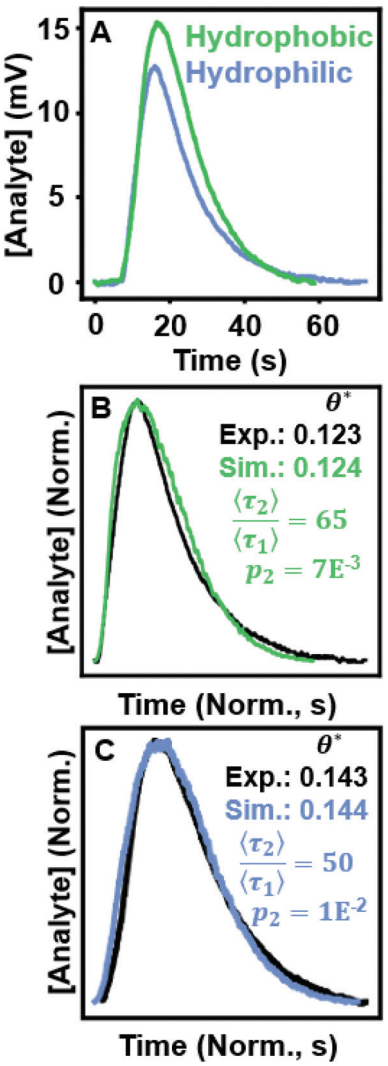

Fig. 6 (A) Chromatograms of lysozyme flowed over hydrophobic and hydrophilic PVDF filters. (B) The hydrophobic experimental data overlaid with a simulated chromatogram $\left(\frac{\langle\tau_2\rangle}{\langle\tau_1\rangle} = 65, p_2 = 0.007\right)$ with θ^* values annotated. (C) The hydrophilic experimental data with an overlaid simulated chromatogram $\left(\frac{\langle\tau_2\rangle}{\langle\tau_1\rangle} = 50, p_2 = 0.01\right)$ with θ^* values annotated.

suggests that the transition from hydrophobic to hydrophilic character decreases the hopping behavior of lysozyme on the stationary phase surface.[100] Increased hopping motion, also called continuous-time random walks, can lead to changes in peak shape.[42] The increase in the prevalence of long interactions on the hydrophilic membrane could also be caused by the increased unfolding of lysozyme on the hydrophilic surface, where the change in surface character introduces a new mode of interaction.[101] Both possibilities represent starting points for imaging of the stationary phase surface to understand the possible chemical moieties that lead to rare surface interactions.

Peak analysis of the hydrophilic surface homogeneous population was performed by removing the contribution of

Published on 02 mis Metheven 2021. Downloaded on 31/05/2026 19:36:48.

interactions with the rare retention mode, a benefit of using simulations. Using methods described by Felinger,[23] we estimate that $\langle \tau_1 \rangle$ = 40 ms if $\langle n \rangle$ = 645 (Fig. S9†). Both values could be scaled to adjust for varied values of $\langle n \rangle$. We can conclude that θ^* would be suitable as a guide for automatically matching experimental chromatograms to simulated data as the analysis only relies on the profile shape, not the chemical identity of the separatory mode or analyte. Simulation/measurement of mobile phase effects would improve the match between peaks as well as refine estimates of $\langle \tau_1 \rangle$ and $\langle n \rangle$, but lies outside the scope of this work.

5. Conclusions

Surface defects and rare chemistries can be detected and estimated using only the ensemble chromatogram. Using the DFR to translate a macroscale chromatogram in terms of microscale surface dynamics offers a route to quality by design rather than quality by testing. Mechanistic insights into the surface allow θ^* to estimate rare retention mode prevalence with higher precision than other commonly used metrics. In absence of microscale surface measurements, θ^* can be supplemented by A_s and skewness to refine the range of possible prevalence/relative desorption time estimates, achieving accurate measurements of surface dynamics using only macroscale data. Using the DFR, experimentally measured ensemble chromatograms can be analyzed to verify if direct observations of retention modes adequately capture qualities of the stationary phase across the whole column. The modular nature of the framework can extend our simulation to include other column effects. Future extensions could include modeling the effects of column construction such as slurry concentration, extra-column broadening effects, and patterned stationary phases. Connecting macroscale chromatograms and microscale surface dynamics directs parameter tuning using surface chemistry rather than phenomenological observations, achieving chemistry-driven design.

Author contributions

Logan D. C. Bishop: Conceptualization, methodology, software, formal analysis, investigation, writing – original draft, writing review & editing. Anastasiia Misiura: Conceptualization, methodology, investigation, validation, resources, writing – original draft. Christy F. Landes: Conceptualization, methodology, visualization, writing – review & editing, supervision, project administration, funding acquisition.

Conflicts of interest

The authors declare no competing financial interest.

Acknowledgements

C. F. L. and A. M. acknowledge the Welch Foundation (Grant C-1787) for support of this work. L. D. C. B. acknowledges that this material is based upon work supported by the National Science Foundation Graduate Research Fellowship Program (Grant 1842494).

References

1 D. G. Sauer, M. Melcher, M. Mosor, N. Walch, M. Berkemeyer, T. Scharl-Hirsch, F. Leisch, A. Jungbauer and A. Dürauer, Real-time monitoring and model-based prediction of purity and quantity during a chromatographic capture of fibroblast growth factor 2, *Biotechnol. Bioeng.*, 2019, **116**(8), 1999–2009.
2 A. S. Rathore, Quality by Design (QbD)-Based Process Development for Purification of a Biotherapeutic, *Trends Biotechnol.*, 2016, **34**(5), 358–370.
3 National Academies of Science, Engineering and Medicine, *A Research Agenda for Transforming Separation Science*, The National Academies Press, Washington, DC, 2019.
4 J. Avorn, The $2.6 Billion Pill - Methodologic and Policy Considerations, *N. Engl. J. Med.*, 2015, **372**(20), 1877–1879.
5 M. Beccaria and D. Cabooter, Current developments in LC-MS for pharmaceutical analysis, *Analyst*, 2020, **145**(4), 1129–1157.
6 R. Kiesswetter, F. Brandl, N. Kastner-Pustet and A. Mannschreck, Chiroptical detection during liquid chromatography: Deconvolution of overlapping peaks of enantiomers and its applications, *Chirality*, 2003, **15**, S40–S49.
7 J. N. Mabry, M. J. Skaug and D. K. Schwartz, Single-Molecule Insights into Retention at a Reversed-Phase Chromatographic Interface, *Anal. Chem.*, 2014, **86**(19), 9451–9458.
8 M. J. Skaug, J. N. Mabry and D. K. Schwartz, Single-Molecule Tracking of Polymer Surface Diffusion, *J. Am. Chem. Soc.*, 2014, **136**(4), 1327–1332.
9 M. J. Wirth and M. A. Legg, Single-molecule probing of adsorption and diffusion on silica surfaces, *Annu. Rev. Phys. Chem.*, 2007, **58**, 489–510.
10 M. J. Wirth and D. J. Swinton, Single-molecule study of an adsorbed oligonucleotide undergoing both lateral diffusion and strong adsorption, *J. Phys. Chem. B*, 2001, **105**(7), 1472–1477.
11 L. Kisley, J. X. Chen, A. P. Mansur, B. Shuang, K. Kourentzi, M. V. Poongavanam, W. H. Chen, S. Dhamane, R. C. Willson and C. F. Landes, Unified superresolution experiments and stochastic theory provide mechanistic insight into protein ion-exchange adsorptive separations, *Proc. Natl. Acad. Sci. U. S. A.*, 2014, **111**(6), 2075–2080.
12 L. Kisley, J. X. Chen, A. P. Mansur, S. Dominguez-Medina, E. Kulla, M. K. Kang, B. Shuang, K. Kourentzi, M. V. Poongavanam, S. Dhamane, R. C. Willson and

 This journal is © The Royal Society of Chemistry 2021

Published on 02 mis Metheven 2021. Downloaded on 31/05/2026 19:36:48.

C. F. Landes, High ionic strength narrows the population of sites participating in protein ion-exchange adsorption: A single-molecule study, *J. Chromatogr. A*, 2014, **1343**, 135–142.
13 A. Cavazzini, F. Dondi, A. Jaulmes, C. Vidal-Madjar and A. Felinger, Monte Carlo model of nonlinear chromatography: correspondence between the microscopic stochastic model and the macroscopic Thomas kinetic model, *Anal. Chem.*, 2002, **74**(24), 6269–6278.
14 F. Dondi, P. Munari, M. Remelli and A. Cavazzini, Monte Carlo model of nonlinear chromatography, *Anal. Chem.*, 2000, **72**(18), 4353–4362.
15 W. Calabrase, L. D. C. Bishop, C. Dutta, A. Misiura, C. F. Landes and L. Kisley, Transforming Separation Science with Single-Molecule Methods, *Anal. Chem.*, 2020, **92**(20), 13622–13629.
16 N. Pamme, Continuous flow separations in microfluidic devices, *Lab Chip*, 2007, **7**(12), 1644–1659.
17 M. Catani, O. H. Ismail, F. Gasparrini, M. Antonelli, L. Pasti, N. Marchetti, S. Felletti and A. Cavazzini, Recent advancements and future directions of superficially porous chiral stationary phases for ultrafast high-performance enantioseparations, *Analyst*, 2017, **142**(4), 555–566.
18 U. J. Wünsch and J. A. Hawkes, Mathematical chromatography deciphers the molecular fingerprints of dissolved organic matter, *Analyst*, 2020, **145**(5), 1789–1800.
19 M. Leśko, J. Samuelsson, E. Glenne, K. Kaczmarski and T. Fornstedt, Predictions of overloaded concentration profiles in supercritical fluid chromatography, *J. Chromatogr. A*, 2021, **1639**, 461926–461937.
20 P. Vajda and G. Guiochon, The modeling of overloaded elution band profiles in supercritical fluid chromatography, *J. Chromatogr. A*, 2014, **1333**, 116–123.
21 F. Gritti, A. Felinger and G. Guiochon, Overloaded gradient elution chromatography on heterogeneous adsorbents in reversed-phase liquid chromatography, *J. Chromatogr. A*, 2003, **1017**(1–2), 45–61.
22 T. Fornstedt, G. M. Zhong and G. Guiochon, Peak tailing and mass transfer kinetics in linear chromatography, *J. Chromatogr. A*, 1996, **741**(1), 1–12.
23 A. Felinger, Molecular movement in an HPLC column: A stochastic analysis, *LCGC North Am.*, 2004, **22**(7), 642–647.
24 J. C. Giddings, Kinetic Origin of Tailing in Chromatography, *Anal. Chem.*, 1963, **35**(13), 1999–2002.
25 J. L. Excoffier, A. Jaulmes, C. Vidalmadjar and G. Guiochon, Characterization of Small Variations in Profiles of Chromatographic Elution Peaks and Effect of Nonlinearity of Sorption Isotherm, *Anal. Chem.*, 1982, **54**(12), 1941–1947.
26 B. A. Rogers, Z. Wu, B. C. Wei, X. M. Zhang, X. Cao, O. Alabi and M. J. Wirth, Submicrometer Particles and Slip Flow in Liquid Chromatography, *Anal. Chem.*, 2015, **87**(5), 2520–2526.
27 A. Felinger, *Data analysis and signal processing in chromatography*, Elsevier, 1998, vol. 21.
28 Ł. Komsta, Y. Heyden and J. Sherma, *Chemometrics in Chromatography*, CRC Press, Boca Raton, 2018.
29 F. Dondi, Approximation Properties of the Edgeworth Cramer Series and Determination of Peak Parameters of Chromatographic Peaks, *Anal. Chem.*, 1982, **54**(3), 473–477.
30 A. Gergely, P. Horvath and B. Noszal, Deconvolution of composite chromatographic peaks by simultaneous dual detections, *J. Chromatogr. Sci.*, 2000, **38**(10), 425–429.
31 O. Trapp, Chromatographic peak deconvolution of constitutional isomers by multiple-reaction-monitoring mass spectrometry, *J. Chromatogr. A*, 2010, **1217**(7), 1010–1016.
32 J. J. Baeza-Baeza, M. J. Ruiz-Angel, M. C. Garcia-Alvarez-Coque and S. Carda-Broch, Half-width plots, a simple tool to predict peak shape, reveal column kinetics and characterise chromatographic columns in liquid chromatography: state of the art and new results, *J. Chromatogr. A*, 2013, **1314**, 142–153.
33 M. F. Wahab, D. C. Patel and D. W. Armstrong, Peak Shapes and Their Measurements: The Need and the Concept Behind Total Peak Shape Analysis, *LC GC Eur.*, 2017, **30**(12), 670–678.
34 L. Mockl and W. E. Moerner, Super-resolution Microscopy with Single Molecules in Biology and Beyond-Essentials, Current Trends, and Future Challenges, *J. Am. Chem. Soc.*, 2020, **142**(42), 17828–17844.
35 H. H. Chen, X. H. Xie and T. Y. Chen, Single-molecule microscopy for in-cell quantification of protein oligomeric stoichiometry, *Curr. Opin. Struct. Biol.*, 2021, **66**, 112–118.
36 M. Pan, Y. Zhang, G. Yan and T.-Y. Chen, Dissection of Interaction Kinetics through Single-Molecule Interaction Simulation, *Anal. Chem.*, 2020, **92**(17), 11582–11589.
37 L. D. C. Bishop, A. Misiura, N. A. Moringo and C. F. Landes, Unraveling peak asymmetry in chromatography through stochastic theory powered Monte Carlo simulations, *J. Chromatogr. A*, 2020, **1625**, 461323–461331.
38 H. Rix, Detection of Small Variations in Shape Between Two Chromatographic Peaks, *J. Chromatogr.*, 1981, **204**(JAN), 163–165.
39 H. Rix and J. P. Malenge, Detecting Small Variations in Shape, *IEEE Trans. Syst. Man Cybern.*, 1980, **10**(2), 90–96.
40 J. Roles and G. Guiochon, Precision and accuracy of the gas solid adsorption-isotherms derived by the elution-by-characteristic-points method, *J. Chromatogr.*, 1992, **591**(1–2), 245–265.
41 L. Pasti, A. Cavazzini, A. Felinger, M. Martin and F. Dondi, Single-molecule observation and chromatography unified by levy process representation, *Anal. Chem.*, 2005, **77**(8), 2524–2535.
42 N. A. Moringo, L. D. C. Bishop, H. Shen, A. Misiura, N. C. Carrejo, R. Baiyasi, W. Wang, F. Ye, J. T. Robinson and C. F. Landes, A mechanistic examination of salting out in protein–polymer membrane interactions, *Proc. Natl. Acad. Sci. U. S. A.*, 2019, **116**(46), 22938–22945.
43 K. H. Jensen, A. Valente and H. A. Stone, Flow rate through microfilters: Influence of the pore size distribution, hydrodynamic interactions, wall slip, and inertia, *Phys. Fluids*, 2014, **26**(5), 13.
44 Z. Wu, B. C. Wei, X. M. Zhang and M. J. Wirth, Efficient Separations of Intact Proteins Using Slip-Flow with Nano-

Published on 02 mis Metheven 2021. Downloaded on 31/05/2026 19:36:48.

Liquid Chromatography-Mass Spectrometry, *Anal. Chem.*, 2014, **86**(3), 1592–1598.
45 J. M. Vanson, A. Boutin, M. Klotz and F. X. Coudert, Transport and adsorption under liquid flow: the role of pore geometry, *Soft Matter*, 2017, **13**(4), 875–885.
46 F. Gritti, J. Hochstrasser, A. Svidrytski, D. Hlushkou and U. Tallarek, Morphology-transport relationships in liquid chromatography: Application to method development in size exclusion chromatography, *J. Chromatogr. A*, 2020, **1620**, 460991–461007.
47 C. Salmean and S. Dimartino, 3D-Printed Stationary Phases with Ordered Morphology: State of the Art and Future Development in Liquid Chromatography, *Chromatographia*, 2019, **82**(1), 443–463.
48 U. Tallarek, D. Hlushkou, J. Rybka and A. Holtzel, Multiscale Simulation of Diffusion in Porous Media: From Interfacial Dynamics to Hierarchical Porosity, *J. Phys. Chem. C*, 2019, **123**(24), 15099–15112.
49 U. Tallarek, J. Hochstrasser, F. Ziegler, X. H. Huang, C. Kubel and M. R. Buchmeiser, Olefin Ring-closing Metathesis under Spatial Confinement: Morphology-transport Relationships, *ChemCatChem*, 2021, **13**(1), 281–292.
50 Y. Vanderheyden, K. Vanderlinden, K. Broeckhoven and G. Desmet, Problems involving the determination of the column-only band broadening in columns producing narrow and tailed peaks, *J. Chromatogr. A*, 2016, **1440**, 74–84.
51 F. Gritti, D. Brousmiche, M. Gilar, T. H. Water and K. Wyndham, Kinetic mechanism of water dewetting from hydrophobic stationary phases utilized in liquid chromatography, *J. Chromatogr. A*, 2019, **1596**, 41–53.
52 M. Grabarics, M. Lettow, A. T. Kirk, G. Von Helden, T. J. Causon and K. Pagel, Plate-height model of ion mobility-mass spectrometry, *Analyst*, 2020, **145**(19), 6313–6333.
53 R. Kumarasinghe, T. Ito and D. A. Higgins, Nanoconfinement and Mass Transport in Silica Mesopores: the Role of Charge at the Single Molecule and Single Pore Levels, *Anal. Chem.*, 2020, **92**(1), 1416–1423.
54 G. Ghimire, R. Espinoza, H. Xu, S. Nasaka, N. Kameta, M. Masuda, D. A. Higgins and T. Ito, Diffusion Behavior of Differently Charged Molecules in Self-Assembled Organic Nanotubes Studied Using Imaging Fluorescence Correlation Spectroscopy, *Langmuir*, 2019, **35**(24), 7783–7790.
55 H. Xu, S. Nagasaka, N. Kameta, M. Masuda, T. Ito and D. A. Higgins, Spectroscopic imaging studies of nanoscale polarity and mass transport phenomena in self-assembled organic nanotubes, *Phys. Chem. Chem. Phys.*, 2017, **19**(30), 20040–20048.
56 J. Rybka, A. Höltzel, A. Steinhoff and U. Tallarek, Molecular Dynamics Study of the Relation between Analyte Retention and Surface Diffusion in Reversed-Phase Liquid Chromatography, *J. Phys. Chem. C*, 2019, **123**, 3672–3681.
57 L. D. C. Bishop and C. F. Landes, From a Protein's Perspective: Elution at the Single-Molecule Level, *Acc. Chem. Res.*, 2018, **51**(9), 2247–2254.
58 N. A. Moringo, H. Shen, L. D. C. Bishop, W. Wang and C. F. Landes, Enhancing Analytical Separations Using Super-Resolution Microscopy, *Annu. Rev. Phys. Chem.*, 2018, **69**(1), 353–375.
59 H. B. Liu, J. Jeong, Y. H. Kao and Y. T. Zhang, Characterization of free thiol variants of an IgG1 by reversed phase ultra high pressure liquid chromatography coupled with mass spectrometry, *J. Pharm. Biomed. Anal.*, 2015, **109**, 142–149.
60 A. Cavazzini, M. Remelli and F. Dondi, Stochastic theory of two-site adsorption chromatography by the characteristic function method, *J. Microcolumn Sep.*, 1997, **9**(4), 295–302.
61 A. Felinger, Determination of rate constants for heterogeneous mass transfer kinetics in liquid chromatography, *J. Chromatogr. A*, 2006, **1126**(1–2), 120–128.
62 J. C. Giddings, Kinetic Model for Chromatographic Dispersion and Electrodiffusion, *J. Chem. Phys.*, 1957, **26**(6), 1755–1756.
63 J. C. Giddings, Stochastic Considerations on Chromatographic Dispersion, *J. Chem. Phys.*, 1957, **26**(1), 169–173.
64 K. V. Kumar, S. Gadipelli, B. Wood, K. A. Ramisetty, A. A. Stewart, C. A. Howard, D. J. L. Brett and F. Rodriguez-Reinoso, Characterization of the adsorption site energies and heterogeneous surfaces of porous materials, *J. Mater. Chem. A*, 2019, **7**(17), 10104–10137.
65 M. J. Wirth and D. J. Swinton, Single-molecule probing of mixed-mode adsorption at a chromatographic interface, *Anal. Chem.*, 1998, **70**(24), 5264–5271.
66 L. Kisley, U. Patil, S. Dhamane, K. Kourentzi, L. J. Tauzin, R. C. Willson and C. F. Landes, Competitive multicomponent anion exchange adsorption of proteins at the single molecule level, *Analyst*, 2017, **142**(17), 3127–3131.
67 J. J. Zhou, M. Q. Wang, B. L. Zhang and Q. Y. Zhang, Metal coordination assisted thermo-sensitive magnetic imprinted microspheres for selective adsorption and efficient elution of proteins, *Colloids Surf., A*, 2021, **612**, 125981–125990.
68 J. C. Giddings and H. Eyring, A Molecular Dynamic Theory of Chromatography, *J. Phys. Chem.*, 1955, **59**(5), 416–421.
69 D. A. Mcquarrie, On Stochastic Theory of Chromatography, *J. Chem. Phys.*, 1963, **38**(2), 437–445.
70 A. Felinger, L. Pasti and F. Dondi, Fourier-Analysis of Multicomponent Chromatograms - Theory and Models, *Anal. Chem.*, 1990, **62**(17), 1846–1853.
71 G. Desmet, A finite parallel zone model to interpret and extend Giddings' coupling theory for the eddy-dispersion in porous chromatographic media, *J. Chromatogr. A*, 2013, **1314**, 124–137.
72 M. J. Wirth, M. D. Ludes and D. J. Swinton, Spectroscopic observation of adsorption to active silanols, *Anal. Chem.*, 1999, **71**(18), 3911–3917.
73 F. Dondi, A. Cavazzini, M. Martin, E. Grushka and S. Lunte, Correspondence between chromatography,

 This journal is © The Royal Society of Chemistry 2021

Published on 02 mis Metheven 2021. Downloaded on 31/05/2026 19:36:48.

single-molecule dynamics, and equilibrium: A stochastic approach, in *Advances in Chromatography*, ed. P. R. Brown, Marcel Dekker, New York, 2005, vol. 43, pp. 179–230.

74 F. Dondi and G. Guiochon, in *Theoretical Advancement in Chromatography and Related Separation Techniques*, Springer Netherlands, 1st edn, 1992.

75 G. J. Mclachlan, S. X. Lee and S. I. Rathnayake, Finite Mixture Models, *Annu. Rev. Stat. Appl.*, 2019, **6**(1), 355–378.

76 D. Hlushkou, A. Svidrytski and U. Tallarek, Tracer-Size-Dependent Pore Space Accessibility and Long-Time Diffusion Coefficient in Amorphous, Mesoporous Silica, *J. Phys. Chem. C*, 2017, **121**(15), 8416–8426.

77 S. Schweiger, S. Hinterberger and A. Jungbauer, Column-to-column packing variation of disposable pre-packed columns for protein chromatography, *J. Chromatogr. A*, 2017, **1527**, 70–79.

78 G. Desmet and K. Broeckhoven, Extra-column band broadening effects in contemporary liquid chromatography: Causes and solutions, *TrAC, Trends Anal. Chem.*, 2019, **119**, 115619–115633.

79 A. E. Reising, S. Schlabach, V. Baranau, D. Stoeckel and U. Tallarek, Analysis of packing microstructure and wall effects in a narrow-bore ultrahigh pressure liquid chromatography column using focused ion-beam scanning electron microscopy, *J. Chromatogr. A*, 2017, **1513**, 172–182.

80 F. Dondi and M. Remelli, The characteristic function method in the stochastic theory of chromatography, *J. Phys. Chem.*, 1986, **90**(9), 1885–1891.

81 Z. Papai and T. L. Pap, Analysis of peak asymmetry in chromatography, *J. Chromatogr. A*, 2002, **953**(1–2), 31–38.

82 M. F. Wahab, D. C. Patel and D. W. Armstrong, Total peak shape analysis: detection and quantitation of concurrent fronting, tailing, and their effect on asymmetry measurements, *J. Chromatogr. A*, 2017, **1509**, 163–170.

83 M. F. Wahab, T. C. O'Haver, F. Gritti, G. Hellinghausen and D. W. Armstrong, Increasing chromatographic resolution of analytical signals using derivative enhancement approach, *Talanta*, 2019, **192**, 492–499.

84 K. J. Millman and M. Aivazis, Python for Scientists and Engineers, *Comput. Sci. Eng.*, 2011, **13**(2), 9–12.

85 S. van der Walt, S. C. Colbert and G. Varoquaux, The NumPy Array: A Structure for Efficient Numerical Computation, *Comput. Sci. Eng.*, 2011, **13**(2), 22–30.

86 P. Virtanen, R. Gommers, T. E. Oliphant, M. Haberland, T. Reddy, D. Cournapeau, E. Burovski, P. Peterson, W. Weckesser, J. Bright, S. J. van der Walt, M. Brett, J. Wilson, K. J. Millman, N. Mayorov, A. R. J. Nelson, E. Jones, R. Kern, E. Larson, C. J. Carey, I. Polat, Y. Feng, E. W. Moore, J. VanderPlas, D. Laxalde, J. Perktold, R. Cimrman, I. Henriksen, E. A. Quintero, C. R. Harris, A. M. Archibald, A. N. H. Ribeiro, F. Pedregosa, P. van Mulbregt and C. SciPy, SciPy 1.0: fundamental algorithms for scientific computing in Python, *Nat. Methods*, 2020, **17**(3), 261–272.

87 A. Felinger, L. Pasti, F. Dondi, M. van Hulst, P. J. Schoenmakers and M. Martin, Stochastic theory of size exclusion chromatography: Peak shape analysis on single columns, *Anal. Chem.*, 2005, **77**(10), 3138–3148.

88 A. Felinger, Molecular dynamic theories in chromatography, *J. Chromatogr. A*, 2008, **1184**(1–2), 20–41.

89 D. Hlushkou, F. Gritti, A. Daneyko, G. Guiochon and U. Tallarek, How Microscopic Characteristics of the Adsorption Kinetics Impact Macroscale Transport in Chromatographic Beds, *J. Phys. Chem. C*, 2013, **117**(44), 22974–22985.

90 D. Hlushkou, F. Gritti, G. Guiochon, A. Seidel-Morgenstern and U. Tallarek, Effect of Adsorption on Solute Dispersion: A Microscopic Stochastic Approach, *Anal. Chem.*, 2014, **86**(9), 4463–4470.

91 K. Horvath, M. Olajos, A. Felinger and P. Hajos, Retention controlling and peak shape simulation in anion chromatography using multiple equilibrium model and stochastic theory, *J. Chromatogr. A*, 2008, **1189**(1–2), 42–51.

92 A. Cavazzini, M. Remelli, F. Dondi and A. Felinger, Stochastic theory of multiple-site linear adsorption chromatography, *Anal. Chem.*, 1999, **71**(16), 3453–3462.

93 A. Savitzky and M. J. E. Golay, Smoothing+differentiation of data by simplified least squares procedures, *Anal. Chem.*, 1964, **36**(8), 1627–1639.

94 F. E. Lytle and R. K. Julian, Automatic Processing of Chromatograms in a High-Throughput Environment, *Clin. Chem.*, 2016, **62**(1), 144–153.

95 K. Broeckhoven, S. Eeltink, W. De Malsche, F. Matheuse, G. Desmet and D. Cabooter, Current and Future Chromatographic Columns: Is One Column Enough to Rule Them All?, *LCGC North Am.*, 2018, **36**(6), 9–17.

96 G. Desmet, D. Cabooter and K. Broeckhoven, Graphical Data Representation Methods To Assess the Quality of LC Columns, *Anal. Chem.*, 2015, **87**(17), 8593–8602.

97 A. F. Kadjo, P. K. Dasgupta and K. Srinivasan, Shape-Based Peak Identity Confirmation in Liquid Chromatography, *Anal. Chem.*, 2021, **93**(8), 3848–3856.

98 J. T. Cooper and J. M. Harris, Imaging Fluorescence-Correlation Spectroscopy for Measuring Fast Surface Diffusion at Liquid/Solid Interfaces, *Anal. Chem.*, 2014, **86**(15), 7618–7626.

99 J. T. Cooper, E. M. Peterson and J. M. Harris, Fluorescence Imaging of Single-Molecule Retention Trajectories in Reversed-Phase Chromatographic Particles, *Anal. Chem.*, 2013, **85**(19), 9363–9370.

100 N. A. Moringo, H. Shen, L. J. Tauzin, W. X. Wang, L. D. C. Bishop and C. F. Landes, Variable Lysozyme Transport Dynamics on Oxidatively Functionalized Polystyrene Films, *Langmuir*, 2017, **33**(41), 10818–10828.

101 J. Hansen, K. Ely, D. Horsley, J. Herron, V. Hlady and J. D. Andrade, The adsorption of lysozymes: A model system. Makromolekulare Chemie, *Macromol. Symp.*, 1988, **17**(1), 135–154.